Human iPSC-derived myocardium-on-chip with capillary-like flow for personalized medicine

Bradley W. Ellis,[1] Aylin Acun,[1] U. Isik Can,[2] and Pinar Zorlutuna[1,2,a)]
[1]*Bioengineering Graduate Program, University of Notre Dame, Notre Dame, Indiana 46556, USA*
[2]*Aerospace and Mechanical Engineering Department, University of Notre Dame, Notre Dame, Indiana 46556, USA*

(Received 21 November 2016; accepted 27 February 2017; published online 16 March 2017)

The heart wall tissue, or the myocardium, is one of the main targets in cardiovascular disease prevention and treatment. Animal models have not been sufficient in mimicking the human myocardium as evident by the very low clinical translation rates of cardiovascular drugs. Additionally, current *in vitro* models of the human myocardium possess several shortcomings such as lack of physiologically relevant co-culture of myocardial cells, lack of a 3D biomimetic environment, and the use of non-human cells. In this study, we address these shortcomings through the design and manufacture of a myocardium-on-chip (MOC) using 3D cell-laden hydrogel constructs and human induced pluripotent stem cell (hiPSC) derived myocardial cells. The MOC utilizes 3D spatially controlled co-culture of hiPSC derived cardiomyocytes (iCMs) and hiPSC derived endothelial cells (iECs) integrated among iCMs as well as in capillary-like side channels, to better mimic the microvasculature seen in native myocardium. We first fully characterized iCMs using immunostaining, genetic, and electrochemical analysis and iECs through immunostaining and alignment analysis to ensure their functionality, and then seeded these cells sequentially into the MOC device. We showed that iECs could be cultured within the microfluidic device without losing their phenotypic lineage commitment, and align with the flow upon physiological level shear stresses. We were able to incorporate iCMs within the device in a spatially controlled manner with the help of photocrosslinkable polymers. The iCMs were shown to be viable and functional within the device up to 7 days, and were integrated with the iECs. The iCMs and iECs in this study were derived from the same hiPSC cell line, essentially mimicking the myocardium of an individual human patient. Such devices are essential for personalized medicine studies where the individual drug response of patients with different genetic backgrounds can be tested in a physiologically relevant manner. *Published by AIP Publishing.*
[http://dx.doi.org/10.1063/1.4978468]

I. INTRODUCTION

Cardiovascular diseases (CVDs) are the leading cause of death in the United States, killing approximately one person every 40 s and costing the U.S. healthcare system $315.4 billion in 2010 alone.[1,2] Furthermore, nearly 50% of CVD related deaths result from myocardial infarction (MI).[1,2] Accordingly, there is an immense amount of ongoing research across various disciplines to prevent and treat CVDs.[3–5] As the first step towards preventing and treating these diseases, understanding the healthy and pathological states of the cardiovascular system (CVS) is crucial. However, the complexity of such an interconnected system brings about many challenges in understanding CVDs.

[a)]Author to whom correspondence should be addressed. Electronic mail: pinar.zorlutuna.1@nd.edu

Most of our current knowledge on how the constituents of the CVS operate to keep the system functioning has been obtained from animal models. Similarly, much of our understanding on the CVS pathophysiology comes from carefully manipulated animal models that possess a desired disease phenotype. However, this disease phenotype is not always attained in a physiologically realistic manner. For example, many murine models of MI utilize either cryoinjury[6–8] or ligation of the coronary artery[9,10] to induce the desired phenotype. In addition, it has become routine to create animal models that overexpress or are devoid of certain genes.[11–14] Since there are many uncontrolled parameters ranging from early developmental factors to influences from other tissues during or after the onset of the disease (e.g., a knocked-down transcription factor affecting a seemingly unrelated gene in a neighboring tissue), it is not uncommon to see contradictory outcomes from independent experiments. Although these experiments usually have carefully selected control groups, it is still quite possible to not take into consideration all the potential variables leading to confounding of the experiments. Such platforms, although indispensable for understanding tissue-level phenomena and systemic aspects of the CVS *in vivo*, require substantial amounts of time, money, and effort. Furthermore, due to the differences in human and animal physiology and pathology, there are often discordances between animal studies and human trials leading to poor success in translating treatments to the clinical setting, with cardiovascular drugs in clinical trials still having a less than 10% likelihood of approval, and many approved drugs being pulled due to cardiotoxicity.[15–18]

As an alternative to animal studies, efforts have been focused on utilizing tissue engineering techniques to fabricate model tissues.[17–22] These model tissues allow for controlled, high-throughput investigation of physiological and pathological phenomena on local levels where systemic influences seen in *in vivo* models could be antagonistic. Furthermore, these engineered models facilitate direct testing on human tissue-like structures, which are invaluable for discovering preventive approaches or treatments. Many current *in vitro* models, where implantation is the goal, utilize biodegradable hydrogels, scaffolds, and decellularized tissue that provide a 3D environment for the cardiomyocytes that mimic their native physiological environment.[17,20–26] In addition, the concept of bioprinting has recently been combined with many of the hydrogels to provide printable cardiac tissue in a controllable geometry and gelation.[17,19,27] Other models, deemed "organs-on-chips," use micropatterned or microwell structures to study the physiological, mechanical, and electrochemical properties of the engineered tissues for better understanding of their *in vivo* abilities.[20–22,27–29] However, the lack of an *in vivo*-like dynamic fluidic environment is a major drawback for many organs-on-chips.[27–29] Microfluidic technologies have recently established themselves as a remedy to this inherent problem of *in vitro* culture. With dimensions in the scale of capillary networks that allow fluid flow in a manner similar to native microvasculature, microfluidics are uniquely well suited for recreating the tissue microenvironment. Additionally, this technology can be manipulated to control the diffusion rates of various molecules including drugs and gases in the microenvironment.[20–22,30–32] As such, several groups have utilized microfluidics to create organs-on-chips that better mimic the local microenvironment found in the native counterpart of the targeted tissue.[17–22,27,33–36]

Although there have been many recent advancements in cardiac tissue engineering, several hurdles still persist. Many models and/or devices are created for a specific use with most efforts focused on implantation,[17,23–27] pharmaceutical screening,[18,27,35–37] tissue/cellular characterization,[28,33,34] or a combination of the three[17,20–22,29] with few focusing on modeling CVS *in vitro*. Additionally, a small percentage of these microfluidic devices have utilized human induced pluripotent stem cells (hiPSCs) as a source of cardiomyocytes for CVD studies.[21,25,32,34] To our knowledge, there are no cardiovascular microfluidic models that utilize completely iPSC-derived cell based co-culture methods to accurately portray physiological conditions of the myocardium, using cells with the same genetic background.

In this study, we first characterized the human iPSC-derived cardiomyocytes (iCMs) and endothelial cells (iECs) derived from the same cell line. We then designed and engineered a human myocardium model as a platform that could be used for studying various aspects of heart disease. We used the characterized iCMs and iECs in this spatially controlled co-culture system to mimic 3D human cardiac muscle and surrounding microvasculature. We then

characterized the myocardium model through viability, alignment, and immunostaining analysis of the hiPSC derived myocardial cells. The novel myocardium-on-a-chip (MOC) we designed and fabricated in this study is the first device that utilizes iCMs and iECs, two cell types native to heart tissue, derived from the same cell source to mimic a patient's native myocardium.

II. MATERIALS AND METHODS

A. Cell culture

1. hiPSC culture

1016 line hiPSCs that were derived from human skin were seeded and maintained on Geltrex (1%, Invitrogen, USA) coated culture flasks in mTeSR1 media (StemCell Technologies, Canada) supplemented with penicillin and streptomycin (P/S) (1%, Life Technologies, USA). hiPSCs were detached using Accutase (StemCell Technologies, Canada), at approximately 80% confluency, and seeded onto glass coverslips (ChemGlass, USA) with Rho-associated, coiled-coil containing protein kinase (ROCK) inhibitor (5 μM, StemCell Technologies, Canada) supplemented mTeSR1. The culture was maintained with daily media changes until 95% confluency was reached.

2. iCM differentiation induction

iCM differentiation induction was adapted from a previously established protocol.[38] Briefly, first the hiPSCs were treated with RPMI Medium 1640 (Life Technologies, USA) supplemented with B27 without insulin (2%, Invitrogen, USA), beta-mercaptoethanol (3.4×10^{-4}%, Promega, USA) and P/S (1%) (CM(−)) with the addition of Wnt activator CHIR99021 (CHIR) (10 μM, Stemgent, USA). Twenty-four hours after (day 2) media was changed to CM(−) without any CHIR. On day 4, iCMs were treated with Wnt inhibitor IWP-4 supplemented CM(−) media (10 μM, Stemgent, USA). Media was then changed back to CM(−) without any small molecules on day 6. On day 9, medium was changed to RPMI Medium 1640 supplemented with B27 (2%, Invitrogen, USA), beta-mercaptoethanol (3.4×10^{-4}%), and P/S (1%) (CM(+)). From day 9-on media was changed every 3 days, and beating was observed as early as day 12 and routinely by day 21 of differentiation. On day 21, iCMs were passaged using trypsin-EDTA (0.25%, Corning, USA) and reseeded on fibronectin in phosphate-buffered saline (PBS) (50 μg/ml, Sigma-Aldrich, USA) coated glass cover slips (ChemGlass, USA) and maintained in Dulbecco's Modified Eagle Medium (Hyclone, USA, DMEM) supplemented with fetal bovine serum (10%, Hyclone, USA, FBS) and P/S (1%) (DMEM complete).

3. iEC differentiation induction

iEC differentiation induction was performed using a previously established protocol.[39] Briefly, on day 1 of the differentiation, hiPSCs were treated with a 1:1 mixture of DMEM to F12 with Glutamax and Neurobasal media supplemented with N2 (Life Technologies, USA), B27, CHIR (8 μM) and bone morphogenic protein 4 (25 ng/ml, R&D Systems, USA). On day 4, the media was replaced with StemPro-34 SFM medium (Life Technologies, USA) supplemented with vascular endothelial growth factor (200 ng/ml, PeproTech), and forskolin (2 μM, Sigma-Aldrich, USA) with medium being renewed again on day 5. At the end of day 6, the cells were sorted against vascular endothelial cadherin (VE-Cad) (Abcam, United Kingdom) with magnetic assisted cell sorting (MACS) using an autoMACSpro (Miltenyi Biotec, Germany, Harvard University). Fluorescence assisted cell sorting was then used to determine the purity of the cell population, which consistently gave more than 95% purity (data not shown).[36] iECs were then cultured on fibronectin coated tissue culture flasks in endothelial growth media-plus (Lonza, Switzerland, EGM+). Human Umbilical Cord Vein Endothelial Cells (HUVECs) were used as positive controls in iEC studies under flow conditions.

B. Immunostaining

Immunostaining was performed on the monolayer cell culture and in the MOC. For MOC immunostaining, solutions were introduced gently by hand through the side channels and allowing for diffusion into the central channel. Cells were washed with PBS (Corning, USA) and fixed with paraformaldehyde (4%, Electron Microscopy Sciences, USA) for either 15 min (for 2D immunostaining) or 1 h (for MOC immunostaining) at room temperature, and then washed with PBS. Cells were then permeabilized in Triton X-100 (0.1%, Sigma-Aldrich, USA) for 30 min and then washed with PBS. Cells were blocked with goat serum (10%, Sigma-Aldrich, USA) for 2 h. After blocking, cells cultured in monolayer were incubated with CD31 (BD Pharmingen, USA), VE-Cad, troponin-I (Abcam, United Kingdom), or connexin-43 (Abcam, United Kingdom) primary antibody diluted (1:100) in goat serum at 4 °C overnight. For the MOC, cells were incubated with VE-Cad or troponin-I primary antibody diluted (1:100) in goat serum at 4 °C overnight. The next day, for all cultures, cells were washed with PBS and then incubated with either Alexa Fluor 594 (Life-Technologies, USA) or Alexa Fluor 488 (Life-Technologies, USA) secondary antibody diluted (1:200) in goat serum at 4 °C for 6 h. After incubation, cells were washed with PBS once and then incubated with DAPI (1:1000 DAPI:PBS, Sigma Aldrich, USA) and then washed with PBS until no background was seen. Imaging was then performed using a confocal microscope (Nikon Confocal Ni-E Upright Research Microscope, Japan) at the Notre Dame Integrated Imaging Facility for monolayer cells or a fluorescence microscope for the MOC (Axio Observer.Z1, Zeiss, Germany, Hamatsu C11440 digital camera, Japan). Post imaging processing was performed using NIS-Elements (Nikon) imaging software (confocal) or provided Zeiss Zen software (fluorescence microscope).

C. Real time Reverse Transcription Polymerase Chain Reaction (RT-PCR)

Total RNA was isolated from confluent (>95%) beating and non-beating (immature) iCMs as well as from confluent (>95%) hiPSCs using the RNAeasy Plus Mini Kit (Qiagen, Germany) and their respective complementary DNA (cDNA) was then synthesized using the Bio-Rad iScript cDNA synthesis kit as per manufacturer's instructions. Gene expression of myosin heavy chain 6 (*MHC6*) (Bio-Rad, USA, MHC), homeobox Nkx2-5 (*NKX2*) (Bio-Rad, USA), and cardiac muscle troponin T (*TNNT2*) (Bio-Rad, USA) were quantified from 1.5 μl of template cDNA using Bio-Rad SYBR Green as per manufacturer's instructions. All assays were performed in triplicate on a CFX Connect Real-Time PCR System (Bio-Rad, USA). Analysis was performed using the CFX Manager Software (Bio-Rad, USA). Gene expression levels were calculated using the ΔC_T and normalized to GAPDH (Eurofin, Luxembourg) as a control.

D. Microelectrode array (MEA) assay

MEAs in this study consisted of poly(3,4-ethylenedioxythiophene) carbon nanotube (PEDOT-CNT) electrodes with a diameter of 30 μm and spaced 200 μm apart (Multichannel Systems, Germany). On day 21, iCMs were trypsinized and seeded onto a fibronectin in PBS coated (50 μg/ml) MEA and supplemented with DMEM complete with media changes every third day until the recommencement of beating. Once beating recommenced, electrical field potentials from the electrodes were measured using MEA-2100 headstage (Multichannel Systems, Germany). Briefly, the MEAs were placed onto the headstage to read the electrical signals through the contact pads of the MEAs. The signals were read by headstage pins and transferred to a computer using the interface board. A temperature controller unit (TC02, Multichannel Systems, Germany) was used to keep the temperature constant at 37 °C throughout the experiments. Cells were stimulated with $\pm$1000 μV, 1 ms biphasic pulses at a frequency of 0.5 Hz. Biphasic pulses were achieved by using two electrodes simultaneously for stimulations. Finally, data sets were exported and plotted using MATLAB. For spontaneous activity data, each individual action potential was detected by a certain threshold and plotted together using this data point as a timestamp. On the other hand, stimulation measurements were plotted by using the stimulation instant (known since the frequency is set by the user input) as the

timestamp. Conduction velocity was calculated by dividing the distance between electrodes by the time it took for the action potential to move between the electrodes.

E. Calcium flux assay

In order to assess the calcium flux of iCMs, media was removed from the iCMs in culture and washed with PBS. Cells were then incubated for 30 min at 37 °C in a calcium sensitive dye, Fluo 4 AM (Thermo Fischer Scientific, USA), prepared following manufacturer's instructions. After 30 min incubation with the Fluo 4 solution, the cells were incubated in warm DMEM complete for an additional 30 min at 37 °C. Real-time imaging was performed using a fluorescence microscope (Axio Observer.Z1, Zeiss, Hamatsu C11440 digital camera) at 50 ms exposure for 1 min with post imaging processing performed using the Zeiss Zen software. Data sets were imported into MATLAB and plotted. For flux activity data, each individual flux was detected by a certain threshold and plotted together using this data point as a timestamp. Time to peak was then calculated using this timestamp and 50% and 90% decay times were then calculated using the peak time as the starting time.

F. Microfluidic device fabrication

1. Master fabrication

Master fabrication was performed at the cleanroom facility of the University of Notre Dame Nanofabrication Facility.

In order to create masters for the 3-channel and 1-channel devices, SU-8 2075 (MicroChem Corp., USA) photoresist was spin coated (1500 rpm, 300 rpm/s, 30 s) at a thickness of $160 \pm 20\ \mu$m on a silicon (Si) wafer. The wafer was soft baked for 10 min at 65 °C and 45 min at 95 °C followed by UV exposure through a transparency mask (Advanced Reproductions, USA) using a mask aligner (Karl Suss MJB-3), and then was developed using SU8 developer (MicroChem Corp., USA).

2. Device fabrication

To fabricate the MOC, polydimethylsiloxane (PDMS) (Corning, USA) was mixed at a 10:1 base to curing agent ratio. After mixing, PDMS was left under vacuum to remove air bubbles, and was poured onto the device master and baked at 90 °C for 20 min. After baking, the PDMS was cut out from the master and cleaned using isopropanol. A glass microscope slide with a thickness of 0.13–0.17 mm (Ted Pella, USA) was cleaned with methanol and both the slide and PDMS were exposed to air plasma using a Dyne-A-Mite air plasma surface treater (Enercon, United Kingdom) for 1 min, and then both surfaces were bonded together and baked at 90 °C for 15 min to complete bonding.

G. MOC preparation

1. iCM encapsulation

Upon fabrication of the devices, the devices were placed in a biosafety cabinet for 1 h for UV sterilization. The iCMs were trypsinized and resuspended at a density of 1.4×10^7, 2.8×10^7, or 4.0×10^7 cells/ml in PBS. A photocrosslinkable hydrogel was used to spatially control the encapsulated iCMs and confine them to the middle channel of the device. To use as the photocrosslinkable hydrogel, UV crosslinkable methacrylated gelatin (GelMA) was synthesized from bovine skin gelatin (Sigma-Aldrich, USA) by addition of methacrylic anhydride (Sigma-Aldrich, USA) to a methacrylation of 80% using previously described methods.[40] The encapsulation procedure was modified from methods previously described.[41] Briefly, to encapsulate the cells, 10% GelMA solution with 0.1% photoinitiator (PI) (BASF, USA) was mixed 1:1 with the resuspended cells (final cell density was between 7×10^6 and 2×10^7cells/ml, final GelMA concentration of 5%, final PI concentration of 0.05%). An excess amount of the GelMA-cell mixture (approximately 100 μl for each device) was perfused by hand through the devices to avoid bubble formation, and the GelMA solution was crosslinked with a brief UV irradiation (6.9 mW/cm^2) of 20 s. Prior to exposure, the side channels were covered with an aluminum foil to prevent crosslinking of

the hydrogel precursor in the side channels. After the exposure, the uncrosslinked GelMA in the side channels was removed by perfusing DMEM through the side channels of the device immediately after crosslinking, leaving the crosslinked cardiac muscle construct only in the cardiac muscle channel. The device was then connected to a syringe pump, and DMEM was perfused through both side channels at a rate of 150 μl/h for 1 h to remove excess PI. The device was kept under static conditions in DMEM overnight. For live co-culture imaging of iCMs and iECs, iCMs were marked using Cell Tracker Red (Life-Technologies, USA). As controls, iCM-laden gel constructs were seeded outside of the MOC on glass at the densities described, and cultured in DMEM.

2. iEC seeding

The day after encapsulation, fibronectin in PBS (50 μl/ml) was introduced carefully by hand into the side channels for 1 h at 37 °C. The iECs were trypsinized and resuspended at a density of 3.0×10^7 cells/ml in EGM+. Approximately 100 μl of the suspended iECs was perfused carefully by hand through the device and kept under static conditions in EGM+ for 24 h to allow for iECs attachment. For live co-culture imaging of iCMs and iECs, iECs were marked using Cell Tracker Green (Life-Technologies, USA).

3. Introduction of capillary-like flow to MOC

24 h after iEC seeding, the device was connected to a syringe pump and EGM+ was perfused through both side channels at a rate of 6 μl/h (giving a wall shear stress of 3 dynes/cm^2) for up to 120 h.

H. Live dead assay

In order to assess the viability of the cells constituting the MOC, Live/Dead assay (Life Technologies, USA) was performed on days 1, 3, and 7 after device seeding. Briefly, the Live/Dead solution was prepared per manufacturer's instructions, perfused into the device, and incubated for 30 min at 37 °C. After incubation, z-stacks of the MOC were imaged using a fluorescence microscope (Axio Observer.Z1, Zeiss, Hamatsu C11440 digital camera). Viability analysis was performed on NIH ImageJ software.

I. Alignment analysis

Images of iECs and the control cells, HUVECs, seeded into single channel devices were taken at 0, 24, and 48 h after the start of perfusion. Additionally, images of the side channels of the MOC were taken on day 7 (5 days after the start of perfusion). Images were then analyzed for alignment using the Directionality plugin for ImageJ software. After analysis, the percentage of cells at each angle of alignment was graphed, with an angle of 0° being the perfect alignment. Additionally, data on the percentage of aligned cells (between −45° and 45°) was graphed.

J. Statistical analysis

The mean ± standard deviation (SD) was reported for all replicates. One-way analysis of variance (ANOVA) followed by Tukey's post hoc analysis was used to find any statistically significant differences. $p < 0.05$ was considered statistically significant.

III. RESULTS

A. MOC design and fabrication

hiPSCs were differentiated into either iECs or iCMs and seeded into different compartments of the MOC. Figure 1(a) summarizes the differentiation, encapsulation, and seeding process for the hiPSC derived iCMs and iECs. iCMs and iECs were utilized to mimic the human cardiac muscle and the surrounding microvasculature, respectively. A three-channel device with 160 μm channel depth was fabricated in order to construct the MOC (Figure 1(b)). Circular posts were

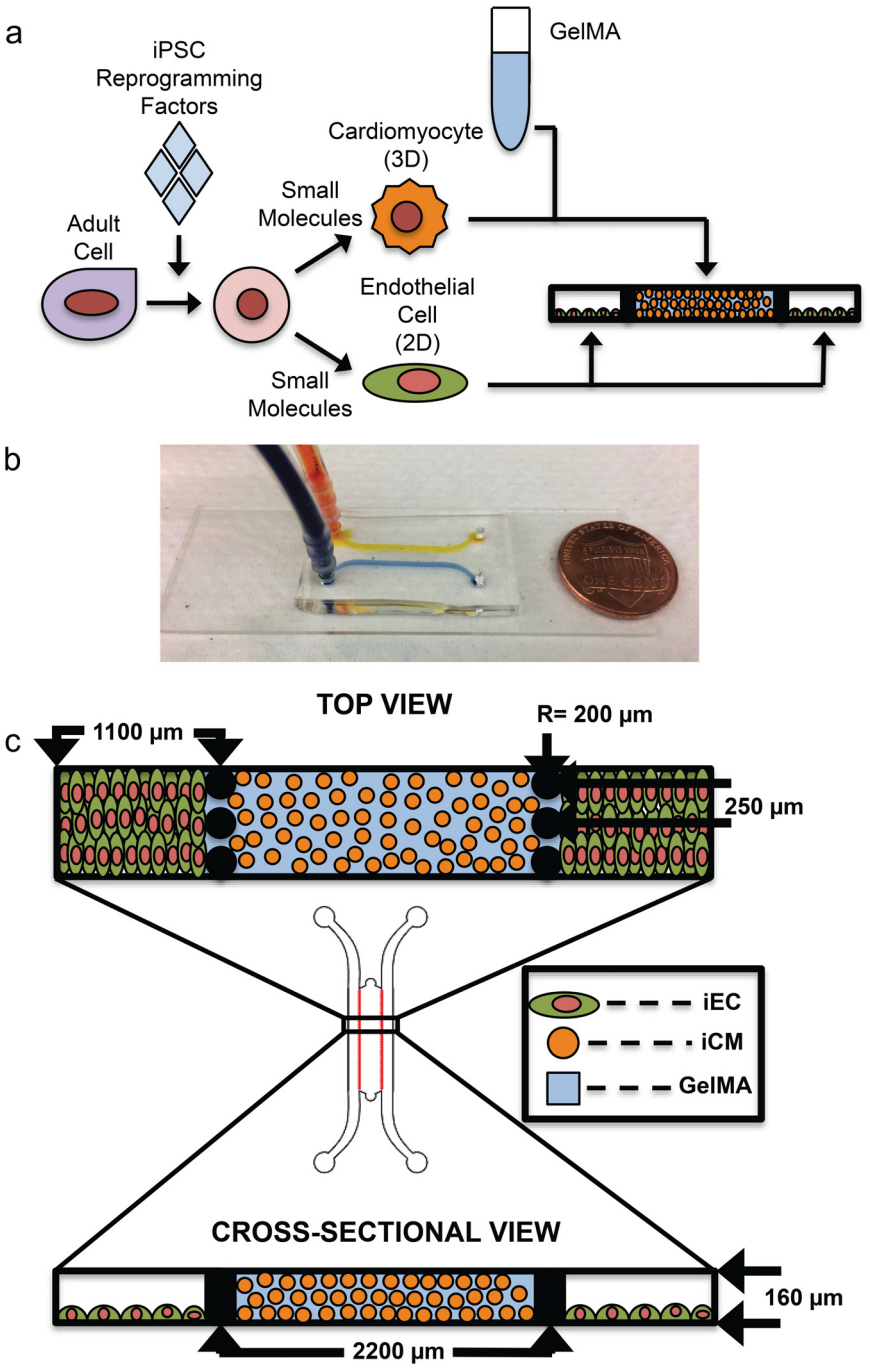

FIG. 1. Experimental plan and schematic of microfluidic Myocardium-on-a-Chip. (a) Adult cells are treated with reprogramming factors to dedifferentiate into hiPSCs. hiPSCs were then redifferentiated into iCMs and iECs and seeded into the MOC (160 μm high) with iCMs being encapsulated in UV-activated GelMA. (b) Gross Image of MOC with food coloring perfused through the side channels, with U.S. one cent piece for scale. (c) iCMs were encapsulated in UV-activated GelMA and seeded into the cardiac muscle channel (2200 μm wide), iECs were then seeded into the microvasculature channels (1100 μm wide) with posts (R = 200 μm) separating the three channels.

designed to separate the channels and serve as a way for the hydrogel to be contained within the central channel without completely closing off the separate portions of the MOC from each other (Figure 1(c)). The 2.2 mm wide central channel of the device served as the 3D cardiac muscle model through the cell-laden hydrogel component, while the 1.1 mm wide side channels mimic the microvasculature, supplying the tissue with nutrients and oxygen through media flow.

B. Characterization of iCMs

In order to confirm the success of the differentiation protocol,[38] we examined the morphological, phenotypical as well as functional markers of the iCMs derived from hiPSCs (Figure 2(a)). From day 1 to 21 of differentiation, hiPSCs became denser and attained tissue-like appearance as the differentiation completed (Figure 2(b)). Beating of isolated areas of iCMs were seen as early as day 12 (14 beats/min (bpm)) of differentiation, and synchronous beating of cell sheets were seen by day 21 (39 ± 11.53 bpm) (supplementary material, Video 1). In order to purify the iCM population, cells

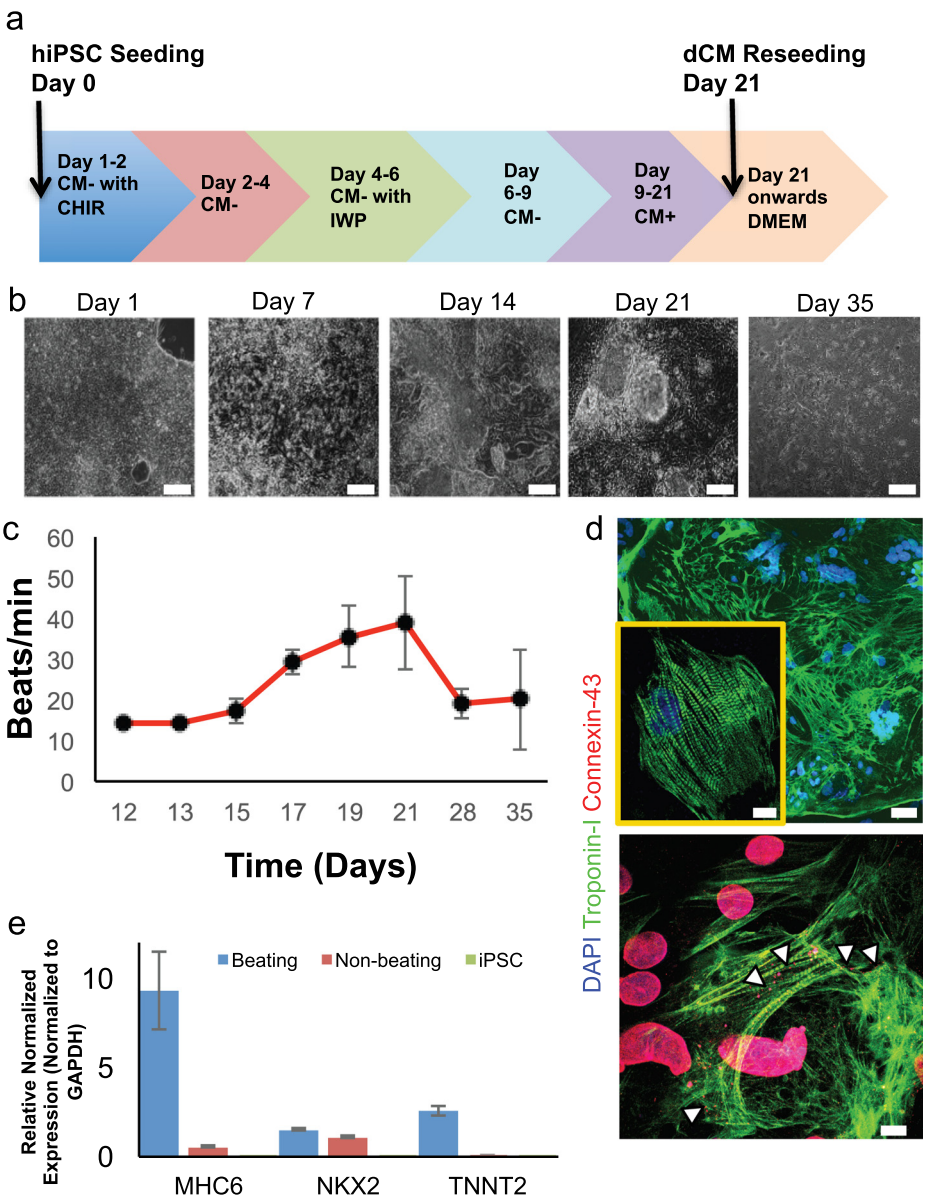

FIG. 2. Biochemical and Physiological Characterization of iCMs. (a) Differentiation and purification plan of iCMs. After differentiation was complete by day 21, iCMs were reseeded in order to purify iCMs and lower hiPSCs present in culture. (b) Brightfield images of hiPSCs as the cells undergo differentiation, throughout differentiation, the hiPSCs condense to become more tissue like. Upon reseeding, iCMs appeared as a synchronously beating monolayer (scale = 200 μm). (c) As the differentiation of hiPSCs to iCMs continued, beating rate of iCMs increased, upon reseeding on day 21 beating ceased, but recommenced by day 28. (d) Fluorescent imaging of reseeded iCMs stained for Troponin-I (top, scale = 50 μm) (inset, scale = 10 μm) and Connexin43 (bottom, scale = 10 μm) on day 35. (e) PCR graph of beating iCMs, non-beating iCMs, and hiPSCs. Completely differentiated iCMs showed a significant upregulation of MHC6, NKX2, and TNNT2 (all $p < 0.05$), with NKX2 levels similar to non-beating iCMs, but higher than hiPSCs ($p < 0.05$).

were reseeded on fibronectin coated substrates on day 21 after synchronous beating of the entire culture was seen (Figure 2(a)). Because hiPSCs need extracellular matrix components such as laminin and collagen to attach to, only differentiated iCMs attached and survived upon seeding on fibronectin-alone coated substrates. Following this reseeding step for their purification, iCMs ceased beating for several days, but beating recommenced as early as 5 days, and spontaneous beating of the entire culture was routinely seen by 14 days after reseeding (20.9 ± 9.33 bpm, supplementary material, Video 2). Additionally, purification caused the dense tissue-like morphology of the iCMs to change to a monolayer of cells phenotypically similar to isolated primary cardiomyocytes (Figure 2(b)) making cellular biochemical and electrophysical analysis possible. Beating frequency of iCMs increased to physiologically relevant levels by day 21 (Figure 2(c)). Once beating recommenced after the reseeding, iCMs displayed a slightly lower beating frequency (Figure 2(c)).

Along with morphology similar to primary cardiomyocytes, reseeded iCMs also exhibited similar protein expression characteristics to primary cardiomyocytes (Figure 2(d)). Two weeks after reseeding, troponin-I expression was filament-like with visible striations, and connexin-43 expression was observed in the cell nucleus and at cell-cell junctions (Figure 2(d)). Messenger RNA (mRNA) expression of beating iCMs showed a significant upregulation ($p < 0.05$) of cardiomyocyte specific markers *MHC6* (9.31 ± 2.17 fold increase), *NKX2* (1.51 ± 0.07 fold increase), and *TNNT2* (2.58 ± 0.28 fold increase) compared to hiPSCs (Figure 2(e)). Additionally, beating iCMs showed a significant upregulation ($p < 0.05$) in *MHC6* and *TNNT2* compared to immature (non-beating reseeded) iCMs (0.57 ± 0.05 and 0.04 ± 0.06 fold increases respectively), but *NKX2* expression of both beating and immature iCMs (1.07 ± 0.06 fold increase) was upregulated at similar levels (Figure 2(e)).

C. Electrophysiological characterization of iCMs

Ca^{2+} ions activate myofilaments and cause contractions in cardiomyocytes.[42] In order to visualize Ca^{2+} transportation during contraction and relaxation periods, Ca^{2+} flux of iCMs was captured using fast Ca^{2+} imaging (supplementary material, Video 3). iCMs displayed a consistent Ca^{2+} flux (Figure 3(a)) with a $16.49 \pm 0.016\%$ increase in fluorescence intensity at peak flux (Figures 3(a) and 3(b)) and a consistent time to peak flux of 185.03 ± 23.52 ms, 50% decay time of 542.59 ± 18.32 ms, and a 90% decay time of 1432.70 ± 37.26 ms (Figure 3(c)). To measure the extracellular membrane potential of the differentiated cells, iCMs were reseeded onto a substrate with MEAs and cultured until beating recommenced (Figure 3(d) and supplementary material, Video 4). Through the membrane potential recordings, the spontaneous beating frequency of the cells was found to be 0.6 Hz (Figure 3(e)) with an extracellular membrane voltage of $92.65 \pm 2.93\,\mu$V (Figure 3(f)). The iCMs also displayed pacing ability through biphasic ± 1000 mV stimulations at a frequency of 0.5 Hz (Figure 3(g)). Conduction velocity of iCMs was calculated to be 4.6 cm/s from the MEA measurements.

D. Functional characterization of iECs

iECs were differentiated from hiPSCs using an established protocol (Figure 4(a)).[39] In previous studies, we have characterized the phenotypical and functional properties of these iEC under static culture conditions.[43] In this study, we seeded iECs into a microfluidic device with a single channel (0.1 mm high $\times$ 1 mm wide $\times$ 10 mm long, Figure 4) to apply physiological-level shear stress and examined the morphology and expression of endothelial cell-specific markers under flow. iECs were seeded into the single-channel microfluidic device (Figure 4(b)) and 24 h after seeding, the device was perfused with culture media up to 72 h. For the first 24 h, the perfusion was kept at a flow rate that corresponded to a wall shear stress of 9.7 dynes/cm^2 which corresponds to average values seen in human capillaries (Figure 4(c)).[44] Within 24 h of perfusion initiation, cells began to align in the direction of flow due to the shear stress applied (Figures 4(c), 4(e), and 4(f)) $53.72 \pm 13.04\%$ of iECs aligned. The shear stress was then increased to 17.8 dynes/cm^2 in order to mimic the above average wall shear stress found in human capillaries.[40] Within 48 h of the flow rate increase, nearly $68.44 \pm 4.31\%$ of iECs were aligned in the direction of the flow (Figures 4(d), 4(e), and 4(f)). 72 h after seeding, we tested if the iECs still expressed endothelial cell markers. We observed that iECs retained the

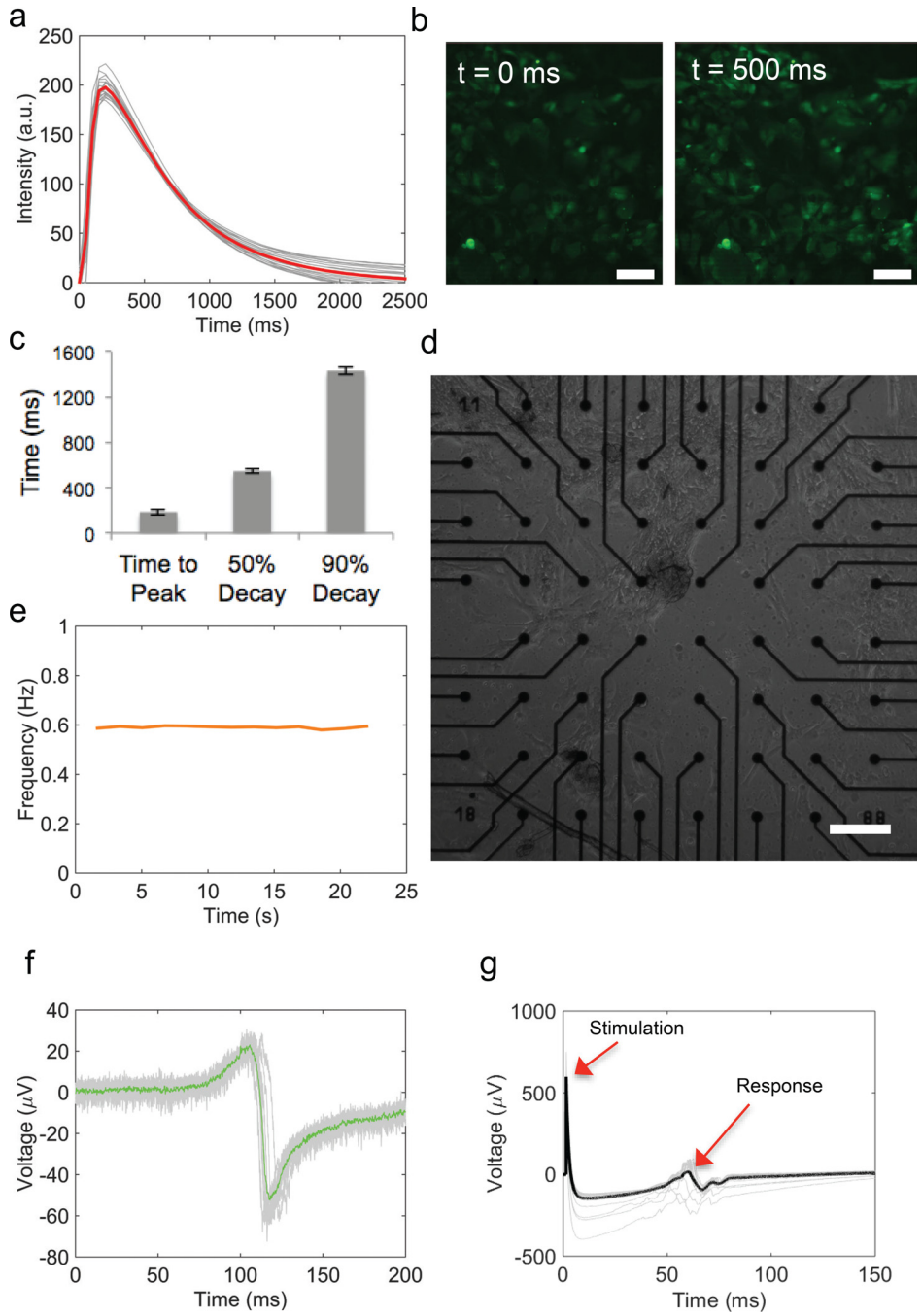

FIG. 3. Electrochemical characterization of iCMs. (a) Intensity of calcium flux timelapse images at 2500 ms intervals. As contraction occurred, intensity increased. (b) Fluorescent image of baseline calcium flux intensity t = 0 ms and at maximum calcium flux t = 500 ms (scale = 100 μm). (c) Time to peak intensity, 50% decay from peak, and 90% decay from peak were calculated for contracting iCMs. (d) Brightfield image of iCMs reseeded onto the MEA for electrophysiological characterization (scale = 200 μm). (e) Reseeded iCMs displayed a consistent, synchronized beating frequency of 0.6 Hz. (f) Spontaneous electric activity of reseeded iCMs, iCMs displayed a membrane surface voltage difference of approximately 80 μV. (g) Stimulation response of reseeded iCMs for ± 1000 mV stimulation at 0.5 Hz, iCMs were able to be paced at this stimulation frequency.

expression of endothelial surface marker CD31 (Figures 4(g) and 4(i)) as well as endothelial adhesion protein VE-Cad (Figures 4(h) and 4(i)). Localization of CD31 and VE-Cad in addition to alignment to flow showed that the iECs function as mature endothelial cells even under physiological shear conditions.

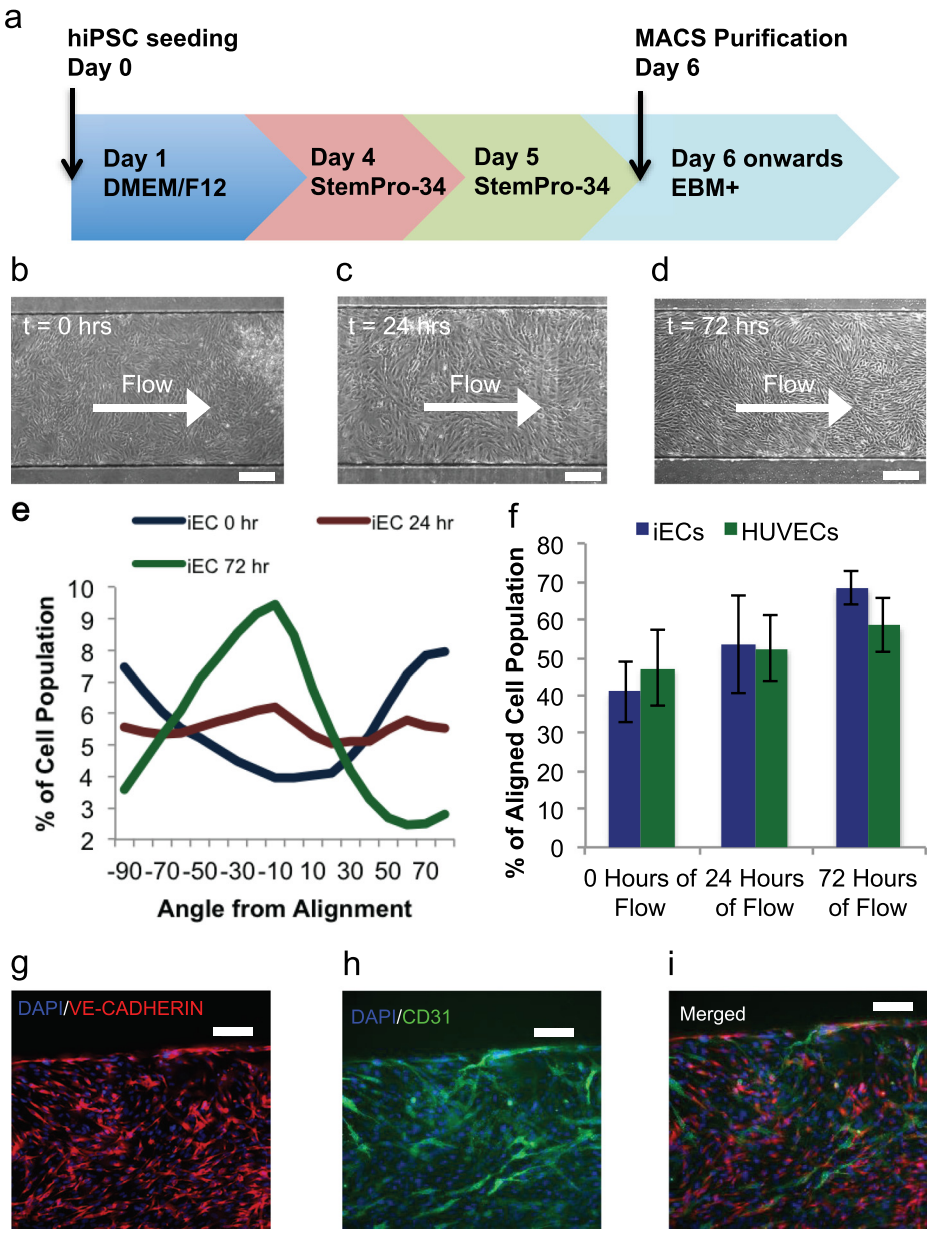

FIG. 4. iEC biochemical and physiological characterization. (a) Differentiation and purification plan of iECs, after differentiation was complete by the end of day 6, cells were purified using magnetic assisted cell sorting. (b) Brightfield image of iECs at initial time of flow (scale = 200 μm). (c) Brightfield image of iECs 24 h after wall shear stress of 9.7 dyne/cm^2 (scale = 200 μm). (d) Brightfield image of aligned iECs 72 h after device perfusion began, with 24 h at a wall shear stress of 9.7 dyne/cm^2 and 48 h at 17.9 dyne/cm^2 (scale = 200 μm). (e) Histogram showing iEC alignment of representative images (b)–(d) at various time points of perfusion. (f) Graph showing the alignment of iECs and HUVECs before, during, and after perfusion. iECs showed a significant ($p < 0.05$) increase in alignment when exposed to physiological wall shear stress for 72 h ($n = 3$ for all). (g) Fluorescent image of aligned iECs stained for endothelial marker VE-Cad 72 h after perfusion (scale = 50 μm). (h) Fluorescent image of aligned iECs stained for endothelial marker CD31 (scale = 50 μm). (i) Merged fluorescent image of aligned iECs stained for CD31 and VE-Cad 72 h after perfusion (scale = 50 μm).

E. MOC characterization

The efficacy of the MOC was characterized using immunofluorescence, alignment analysis, and live/dead analysis (Figures 5(a)–5(i)). iCMs encapsulated in GelMA were successfully seeded into the cardiac muscle chamber of the MOC with a consistent distribution seen throughout the device (Figure 5(a)). The majority of iECs seeded into the MOC attached into the two

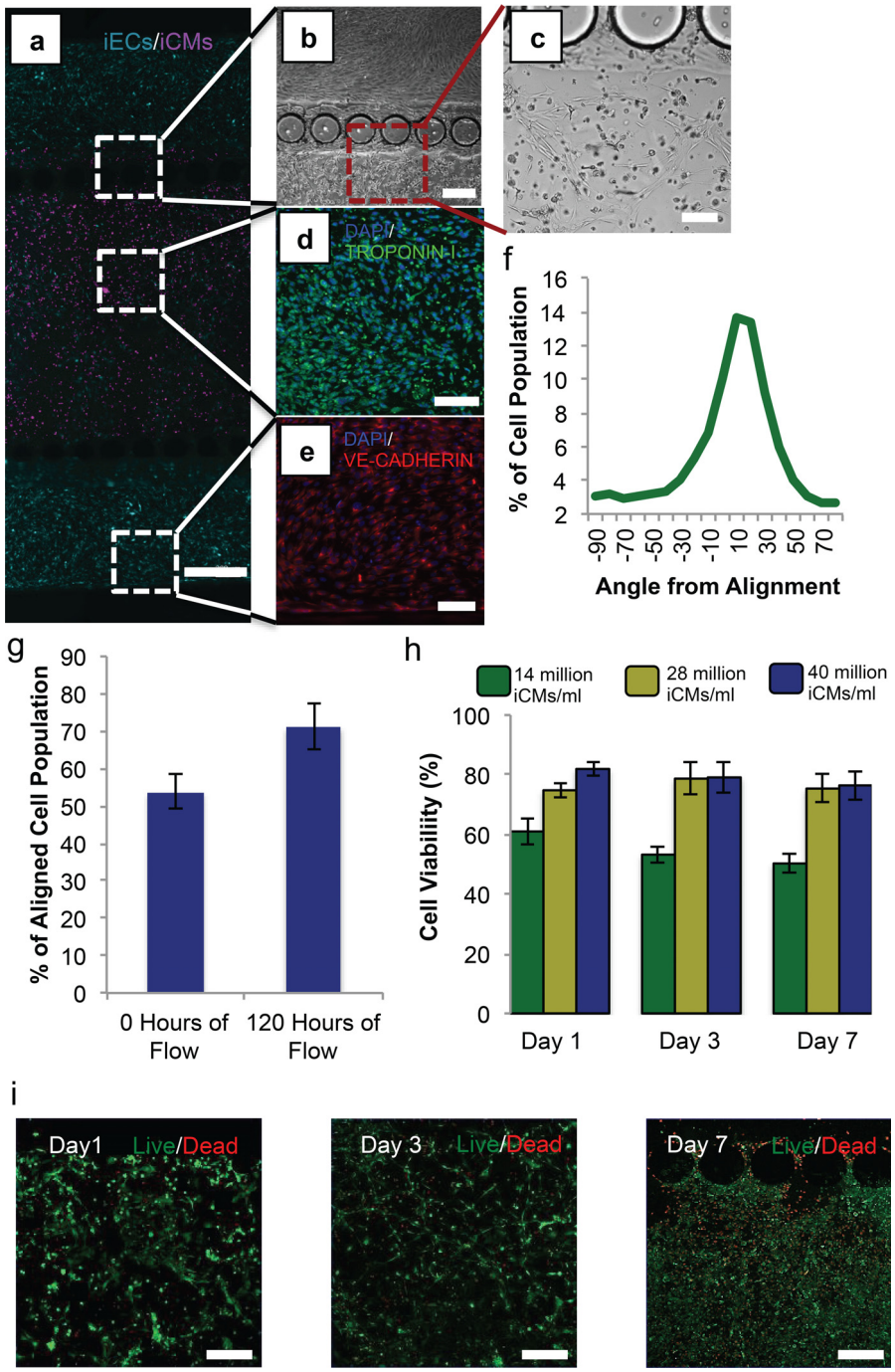

FIG. 5. iCMs and iECs seeded into the MOC retain markers and viability in culture. (a) A seeded MOC with encapsulated iCMs (magenta) in the cardiac muscle channel and iECs (cyan) seeded into the microvasculature channels with iECs additionally seeded into the cardiac muscle channel (scale = 500 μm). (b) Brightfield image of MOC 7 days after culture showing aligned iECs (scale = 250 μm). (c) Brightfield image of MOC's cardiac muscle channel showing iCMs (dense circular cells) and tube formation of iECs (spread out cells) on top of and in the cardiac muscle of the MOC (scale = 100 μm). (d) Fluorescent image of MOC's cardiac muscle channel showing Troponin-I expression of encapsulated iCMs (scale = 100 μm). (e) Fluorescent image of MOC's microvasculature channel showing Ve-Cadherin expression of aligned iECs (scale = 100 μm). (f) Histogram showing iEC angle from the alignment of representative image (b) in the MOC after 7 days in culture. (g) Graph showing a significant increase ($p < 0.05$) in alignment of iECs at day 2 (0 h of perfusion) and day 7 (120 h of perfusion) of culture (n = 3 for all). (h) Viability of iCMs seeded in the myocardium channel over the culture period at varying encapsulation densities (n = 3 for all). (i) Representative z-stack images of iCMs (encapsulation of 40×10^6 iCMs/ml) stained for the live/dead assay at days 1, 3, and 7 days of culture (scale = 200 μm).

microvasculature channels, with some iECs infusing into the middle channel (Figure 5(a)). After cell seeding, we perfused the MOC with EGM+ through both side channels applying a wall shear stress at lower values found in human capillaries (3 dynes/cm^2)[44] and observed that the engineered microvasculature aligned in the direction of flow within 120 h of perfusion (Figures 5(b), 5(f), and 5(g)), with over $71.16 \pm 5.99\%$ of iEC in the microvasculature channel aligned. EGM+ was chosen as the media for both cell types as control experiments with cell-laden gels without the device showed that both iCMs and iECs displayed high survivability in this media (data not show). In addition, the iECs that infused into cardiac muscle chamber integrated into the engineered cardiac muscle tissue, and showed tube-like formations within the hydrogel filling the middle channel (Figure 5(c)). iCMs stopped beating upon encapsulation within the MOC and outside of the device. Five days after encapsulation, spontaneous beating was resumed both in iCM-laden control hydrogel constructs (supplementary material, Video 5) and in the iCMs encapsulated inside the microfluidic device (supplementary material, Video 6). Encapsulated iCMs retained troponin-I expression for up to seven days after encapsulation, with expression appearing to be throughout the entire cytoplasm of the cells (Figure 5(d)). Similarly, the MOC microvasculature expressed VE-Cad for up to seven days, with the protein localized to the cell membrane (Figure 5(e)).

In order to better characterize the efficacy of the device as an *in vitro* model to study the human myocardium, the viability of the cells in the cardiac muscle chamber, the majority of which were encapsulated iCMs (Figure 5(a)), was assessed for seven days in culture. Of the three encapsulation densities tested, the higher encapsulation densities of 28×10^6 iCMs/ml ($75.36 \pm 4.60\%$) and 40×10^6 iCMs/ml ($76.42 \pm 5.03\%$) displayed significantly higher viability ($p < 0.05$) than the lowest encapsulation density of 14×10^6 iCMs/ml ($50.35 \pm 3.17\%$) (Figure 5(h)). For the highest encapsulation density, cell viability remained consistent over the entire time that the devices remained in culture (Figure 5(h)). Moreover, we observed that the live cells were equally distributed throughout the central channel during the 7 days that the devices were maintained in culture (Figure 5(i)). Similarly, the dead cells were equally distributed for the first several days of culture, but by day 7, the majority of dead cells were seen on the ends of the device, where the cardiac muscle and microvasculature channels are separated (data not shown) with an additional relatively large subset seen near the posts of the microfluidic device (Figure 5(i)). Additionally, due to the gas permeable nature of PDMS and shallow (160 μm) depth of the MOC, which is within the oxygen penetration limits, oxygen diffusion was not expected to affect the viability of iCMs and iECs in the MOC.

IV. DISCUSSION AND CONCLUSION

Many recent publications have demonstrated the extent of tissue engineering to study the various aspects of cardiovascular biology.[17–22,27–36] In this study, we showed that hiPSC derived iCMs and iECs are suitable for the engineering of an *in vitro* human myocardium for studying cardiovascular biology and pathophysiology. hiPSCs derived from the same source were successfully differentiated into both functioning cardiomyocytes and endothelial cells to engineer a MOC that can be used for future studies of cardiovascular physiology and disease.

The iCMs in this study displayed biochemical, phenotypic, and functional characteristics similar to native cardiac tissue. At the mRNA level, *NKX2* expression, an early transcription factor in CM differentiation, was significantly upregulated in both immature and mature iCMs. This is in agreement with the normal cardiac development, as *NKX2* encodes for the homeoprotein NKX2-5 that has been shown to be critical in mouse heart development.[45] Additionally, the upregulation of contraction markers *MHC6* and *TNNT2* and spontaneous, synchronized beating confirms that the differentiation of hiPSCs to a contractile cardiomyocyte phenotype was successful, and that these cells could be used to fabricate the MOC. At the protein level, differentiated iCMs showed expressions of both troponin-I and connexin-43. Troponin-I, which is required for contraction, was expressed as striated fibers throughout the entire cell similar to primary cardiomyocytes.[46] The presence of nuclear connexin-43 suggests that iCMs were still not completely mature. However, we also observed non-nuclear connexin-43 that was localized to the cell

membrane where it is essential for iCM-iCM interactions, thus synchronous beating. Protein expression was in agreement with the functionality as the iCMs displayed synchronous contraction before and after reseeding. Morphologically, upon completion of iCM differentiation, cells were tissue-like in appearance, and they were beating at a consistent physiological rate of 39 bpm on average.[42] Upon reseeding, iCMs had a similar appearance to primary isolated cardiomyocytes and retained their consistent beating rate (20.9 bpm on average) comparable to other human iCMs.[47] iCMs also displayed regulated calcium oscillations that were synchronized to contraction. Oscillations displayed slower time to peak and a longer decay time than murine cardiomyocytes, both primary and stem cell derived.[28,48] As murine cardiomyocytes beat at a much higher frequency, this discrepancy in parameters is probably due to species to species variability. However, when compared to other human iCMs studies in literature, our iCMs displayed similar time to peak and 50% decay.[47] Additionally, MEA analysis of the electrophysiological activity of the iCMs showed lower extracellular membrane potential and frequency than primary cardiomyocytes isolated from other mammalian models,[48] and human embryonic stem cell-derived cardiomyocytes.[49] Other studies show that lower calcium transient and electrophysiological activity are commonly observed with hiPSC-derived iCMs.[47] However, the main goal of this study is to develop a functional *in vitro* MOC model where we can compare the baseline measurements to after-treatment measurements. Therefore, the suboptimal electrophysiological characteristics of hiPSC-derived iCMs do not impose a detrimental disadvantage. In addition, the conduction velocity of 4.6 cm/s of the reseeded iCMs was found to be similar to other human and murine iPSC derived cardiomyocytes presented in the literature.[28,48–51] In these studies the conduction velocities, membrane potentials, and calcium flux were calculated on non-purified cells, as well as on murine iCMs.[48,51] With protein, genetic, and phenotypical characterization consistent with those of primary cardiomyocytes and electrical properties comparable to those of previous stem cell derived cardiomyocytes, the human iCMs proved adequate to model the human myocardium in the MOC.

Next, we showed that our hiPSCs were successfully differentiated into iECs through phenotypical and protein characterization. Previous characterizations from our group have shown that cells differentiated using this protocol are very similar to HUVECs in mRNA and protein expression as well as in tube formation ability.[43] In this study, we characterize the cells further under flow. iECs seeded into both the single channel device and the MOC appeared morphologically similar to primary endothelial cells. Additionally, in both platforms, iECs aligned to the direction of flow when exposed to shear flow, consistent with the literature.[52] We observed the expression of typical endothelial markers CD31 and VE-Cad on seeded iECs after perfusion. CD31 was localized to the membrane of endothelial cells consistent with CD31 expression in primary endothelial cells. Moreover, VE-Cad localized to the membrane of iECs, suggesting that it is properly functioning in its role as a cell-cell attachment protein.[53,54] With the proper expression of canonical endothelial markers and the ability to align to wall shear stresses comparable to those seen in human capillary networks, hiPSC derived iECs were successfully used to model the human capillary network of native myocardium in the MOC.

We successfully utilized the iECs and iCMs to model the human myocardium in a spatially controlled microfluidic system that can be used as a model to study human physiology *in vitro* while closely mimicking *in vivo* biology. Both cell types retained their phenotypes and lineage specific functionalities consistent with their respective primary cells for the entirety of the culture period. This allowed us to mimic the microvasculature, with iECs, and cardiac muscle, with iECs and iCMs, of the human myocardium. The formation of tube-like networks of the seeded iECs that infiltrated into the cardiac muscle channel of the MOC allows our device to more closely mimic the microvasculature present in native human myocardium. With longer time in culture and growth factor supplements, this immature network that we observed could be further refined and utilized as a method of transport for cytokines secreted from the iECs or in the cell culture medium, which will be a focus in future studies. Also, our results demonstrated the effect of different iCM encapsulation densities on cell survival in our model system, with increased iCM density improving the viability of the cells in the MOC. This is in line

with both previous studies from our group[43] and by others,[55–58] that show cardiomyocyte-cardiomyocyte and cardiomyocyte-endothelial cell interactions, as well as the distance between cells have a significant effect on cell viability. Increasing the encapsulation density of iCMs decreases the distance between each individual cell and increases cell-cell connections thus, the interactions, and helped increasing the cell viability in the MOC. Most importantly, encapsulated iCMs retained their ability to spontaneously beat, showing that they still function in a way that can properly mimic human myocardium. These results demonstrate the feasibility of the MOC as a supplementary approach to animal and other *in vitro* models to study the pathophysiology and biology of cardiac tissue. In addition, the proposed model allows for the incorporation of genetic modifications to one or more cell types in a controlled manner, which is either difficult or impossible to study in an *in vivo* setting. In subsequent studies, we plan on using these parameters of the MOC to study iCM/iEC interactions and myocardial health under normal and pathological conditions. In addition, we can use these parameters to measure the effect of drug or environmental treatments in a way that can be correlated to results seen in clinical setting.[59]

In contrast to other heart-on-chip models, the MOC possesses the versatility to study various aspects of cardiovascular biology on a single device. Like many other devices[18,20–22,24–26,30–33] the MOC has the potential to measure the contractility of iCMs through image analysis of the cardiac muscle portion. However, due to the encapsulation of iCMs, the contractility measurements would only be in the single cell level, but in future studies, increasing the iCM encapsulation density to increase iCM-iCM interactions and synchronicity would remedy this issue. In addition to contractile measurements, the MOC is capable of analyzing cardiac and endothelial health of the myocardium before and after drug treatment. The addition of iECs into our device design allows for physiologically relevant introduction of drugs and small molecules to the microvascular channels to diffuse into the cardiac muscle, which is not possible in other current heart-on-chip drug screening models.[21,22,27,29,35,36] However, the use of two cell types, does increase the time required for MOC fabrication when compared to other models.[20–22,28,29,33–36] In future studies, we plan on optimizing and manipulating the microvasculature seen in the cardiac muscle portion of the MOC as an additional method of delivery. The use of a 2D vascular and 3D cardiac muscle portion allows for separate removal of each section to isolate the protein expression and gene regulation of either section of the MOC by trypsinzation and removal of the microvasculature followed by digestion and removal of the cardiac muscle. In addition, the 3D aspect of the cardiac muscle channel of the MOC increases iCM-iCM and iCM-iEC interactions[43] and provides iCMs with an extracellular matrix, allowing for a more *in vivo* like environment. The small size and transparency of the MOC also allows for culture in gas and temperature controlled microscopy incubation chambers for observation of real-time effects of drug and environmental treatment.

The MOC that we developed in this study displays a great potential as an engineered microfluidic model mimicking the human myocardium and allowing for the *in vitro* study of cardiovascular phenomena. The device can be used to better scrutinize procedures and drug treatments for CVD before moving on to more costly animal models, and in turn increase the success rate of drugs and procedures that move on to clinical trials. Additionally, with the use of hiPSCs, our device is uniquely suited to allow for the genetic engineering to study specific genes and their role as risk factors for CVD as well as their specific role in the pathophysiology of the heart. Clinically, the MOC could also be further developed as a method for testing the abilities of patient derived iCMs to ensure that they can be used as a cardiac tissue implant. This particular use of the MOC has a great potential in personalized medicine because cells planned for implantation can be genetically modified in accordance to the individual needs, and the MOC can assess the efficacy of these modified cells. While the MOC is currently intended as a tool for *in vitro* analyses, the platform may provide the foundation to future developments of superior tissue engineering constructs for cardiac tissue replacements.

SUPPLEMENTARY MATERIAL

See supplementary material for Video S1 that shows beating iCMs before purification reseeding. Video S2 shows beating iCMs after purification reseeding. Video S3 shows Ca^{2+} imaging of reseeded iCMs. Video S4 shows beating reseeded iCMs on the MEA. Video S5 shows encapsulated iCMs beating in control GelMA. Video S6 shows encapsulated iCMs beating in the fully seeded MOC. Supplementary Video 1. Compressed video of iCMs beating on day 21 of differentiation before reseeding. Supplementary Video 2. Compressed video of reseeded iCMs beating on day 35 of differentiation. Supplementary Video 3. Compressed and trimmed fluorescent timelapse video of beating reseeded dCMs stained for calcium flux analysis two weeks after reseeding. Supplementary Video 4. Compressed and trimmed timelapse video of reseeded beating dCMs on MEA 1 week after reseeding. Supplementary Video 5. Compressed video of beating encapsulated iCMs 5 days after encapsulation in GelMA. Supplementary Video 6. Compressed video of beating encapsulated iCMs 5 days after seeding the iCMs into the MOC.

ACKNOWLEDGMENTS

We thank Dr. C. Cowan, Dr. K. Musunuru, and Dr. L. Challet-Meylan, Harvard University, for providing human induced pluripotent cells and reagents, and for their helpful suggestions and scientific insight on stem cell culture and differentiation. This work was supported by a Project Development Team within the Indiana Clinical and Transitional Sciences Institute, National Institutes of Health/ National Center for Research Resources (ICTSI NIH/NCRR) [Grant No. UL1TR001108], by Advanced Diagnostics and Therapeutics Discovery Grant and by NSF Grant No. 1530884.

[1]M. A. Laflamme and C. E. Murry, "Regenerating the heart," Nat. Biotechnol. **23**(7), 845–856 (2005).
[2]D. Mozaffarian, E. J. Benjamin, A. S. Go, D. K. Arnett, M. J. Blaha, M. Cushman, and M. D. Huffman, "Executive summary," Circulation **131**(4), 434–441 (2015).
[3]S. Kathiresan and D. Srivastava, "Genetics of human cardiovascular disease," Cell **148**(6), 1242–1257 (2012).
[4]B. Lu, H. Yu, M. Zwartbol, W. P. Ruifrok, W. H. van Gilst, R. A. de Boer, and H. H. Silljé, "Identification of hypertrophy and heart failure associated genes by combining in vitro and in vivo models," Physiol. Genomics **44**(8), 443–454 (2012).
[5]K. Sarkar, Z. Cai, R. Gupta, N. Parajuli, K. Fox-Talbot, M. S. Darshan, and G. L. Semenza, "Hypoxia-inducible factor 1 transcriptional activity in endothelial cells is required for acute phase cardioprotection induced by ischemic preconditioning," Proc. Natl. Acad. Sci. U.S.A. **109**(26), 10504–10509 (2012).
[6]J. Jin, S. I. Jeong, Y. M. Shin, K. S. Lim, Y. M. Lee, H. C. Koh, and K. S. Kim, "Transplantation of mesenchymal stem cells within a poly (lactide-co-ε-caprolactone) scaffold improves cardiac function in a rat myocardial infarction model," Eur. J. Heart Failure **11**(2), 147–153 (2009).
[7]E. J. van den Bos, B. M. Mees, M. C. de Waard, R. de Crom, and D. J. Duncker, "A novel model of cryoinjury-induced myocardial infarction in the mouse: a comparison with coronary artery ligation," Am. J. Physiol.-Heart Circ. Physiol. **289**(3), H1291–H1300 (2005).
[8]B. D. Polizzotti, B. Ganapathy, B. J. Haubner, J. M. Penninger, and B. Kühn, "A cryoinjury model in neonatal mice for cardiac translational and regeneration research," Nat. Protoc. **11**(3), 542–552 (2016).
[9]E. Gao, Y. H. Lei, X. Shang, Z. M. Huang, L. Zuo, M. Boucher, and W. J. Koch, "A novel and efficient model of coronary artery ligation and myocardial infarction in the mouse," Circ. Res. **107**(12), 1445–1453 (2010).
[10]J. Wang, H. Bo, X. Meng, Y. Wu, Y. Bao, and Y. Li, "A simple and fast experimental model," Texas Heart Inst. J. **33**(3), 290–293 (2006).
[11]R. Natarajan, F. N. Salloum, B. J. Fisher, and R. C. Kukreja, "Hypoxia inducible factor-1 activation by prolyl 4-hydroxylase-2 gene silencing attenuates myocardial ischemia reperfusion injury," Circ. Res. **98**(1), 133–140 (2006).
[12]R. Natarajan, F. N. Salloum, B. J. Fisher, and R. C. Kukreja, "Hypoxia inducible factor-1 upregulates adiponectin in diabetic mouse hearts and attenuates post-ischemic injury," J. Cardiovasc. Pharmacol. **51**(2), 178–187 (2008).
[13]Y. Higashikuni, J. Sainz, K. Nakamura, M. Takaoka, S. Enomoto, H. Iwata, and H. Kusuhara, "The ATP-binding cassette transporter BCRP1/ABCG2 plays a pivotal role in cardiac repair after myocardial infarction via modulation of microvascular endothelial cell survival and function," Arterioscler., Thromb., Vasc. Biol. **30**(11), 2128–2135 (2010).
[14]M. Skolimowski, M. W. Nielsen, F. Abeille, P. Skafte-Pedersen, D. Sabourin, A. Fercher, and M. Dufva, "Modular microfluidic system as a model of cystic fibrosis airways," Biomicrofluidics **6**(3), 034109 (2012).
[15]S. Young and K. Sutton, "Building an organ on a chip," Technol. Rev. **115**(4), 80–82 (2012).
[16]M. Hay, D. W. Thomas, J. L. Craighead, C. Economides, and J. Rosenthal, "Clinical development success rates for investigational drugs," Nat. Biotechnol. **32**(1), 40–51 (2014).
[17]Y. S. Zhang, J. Aleman, A. Arneri, S. Bersini, F. Piraino, S. R. Shin, M. R. Dokmeci, and A. Khademhosseini, Biomed. Mater. **10**(3), 034006 (2015).
[18]J. Ribas, H. Sadeghi, A. Manbachi, J. Leijten, K. Brinegar, Y. S. Zhang, and A. Khademhosseini, "Cardiovascular organ-on-a-chip platforms for drug discovery and development," Appl. In Vitro Toxicol. **2**(2), 82–96 (2016).

[19]Y. S. Zhang and A. Khademhosseini, "Seeking the right context for evaluating nanomedicine: From tissue models in petri dishes to microfluidic organs-on-a-chip," Nanomedicine **10**(5), 685–688 (2015).
[20]C. S. Simmons, B. C. Petzold, and B. L. Pruitt, "Microsystems for biomimetic stimulation of cardiac cells," Lab Chip **12**(18), 3235–3248 (2012).
[21]E. Jastrzebska, E. Tomecka, and I. Jesion, "Heart-on-a-chip based on stem cell biology," Biosens. Bioelectron. **75**, 67–81 (2016).
[22]H. Yang and Z. Ma, "Microsystem for stem cell-based cardiovascular research," BioNanoScience **2**(4), 305–315 (2012).
[23]G. C. Engelmayr, M. Cheng, C. J. Bettinger, J. T. Borenstein, R. Langer, and L. E. Freed, "Accordion-like honeycombs for tissue engineering of cardiac anisotropy," Nat. Mater. **7**(12), 1003–1010 (2008).
[24]D. Kai, M. P. Prabhakaran, G. Jin, and S. Ramakrishna, "Polypyrrole-contained electrospun conductive nanofibrous membranes for cardiac tissue engineering," J. Biomed. Mater. Res., Part A **99A**(3), 376–385 (2011).
[25]R. A. Neal, A. Jean, H. Park, P. B. Wu, J. Hsiao, G. C. Engelmayr, Jr., and L. E. Freed, "Three-dimensional elastomeric scaffolds designed with cardiac-mimetic structural and mechanical features," Tissue Eng., Part A **19**(5–6), 793–807 (2012).
[26]A. Agarwal, Y. Farouz, A. P. Nesmith, L. F. Deravi, M. L. McCain, and K. K. Parker, "Micropatterning alginate substrates for in vitro cardiovascular muscle on a chip," Adv. Funct. Mater. **23**(30), 3738–3746 (2013).
[27]Y. S. Zhang, A. Arneri, S. Bersini, S. Shin, K. Zhu, Z. Goli-Malekabadi, and A. Khademhosseini, "Bioprinting 3D microfibrous scaffolds for engineering endothelialized myocardium and heart-on-a-chip," Biomaterials **110**, 45–59 (2016).
[28]Y. Aratyn-Schaus, F. S. Pasqualini, H. Yuan, M. L. McCain, J. C. George, S. P. Sheehy, and K. K. Parker, "Coupling primary and stem cell–derived cardiomyocytes in an in vitro model of cardiac cell therapy," J. Cell Biol. **212**(4), 389–397 (2016).
[29]A. Grosberg, P. W. Alford, M. L. McCain, and K. K. Parker, "Ensembles of engineered cardiac tissues for physiological and pharmacological study: Heart on a chip," Lab Chip **11**(24), 4165–4173 (2011).
[30]G. Mehta, K. Mehta, D. Sud, J. W. Song, T. Bersano-Begey, N. Futai, and S. Takayama, "Quantitative measurement and control of oxygen levels in microfluidic poly (dimethylsiloxane) bioreactors during cell culture," Biomed. Microdevices **9**(2), 123–134 (2007).
[31]P. C. Thomas, S. R. Raghavan, and S. P. Forry, "Regulating oxygen levels in a microfluidic device," Anal. Chem. **83**(22), 8821–8824 (2011).
[32]M. Björnmalm, Y. Yan, and F. Caruso, "Engineering and evaluating drug delivery particles in microfluidic devices," J. Controlled Release **190**, 139–149 (2014).
[33]A. Aung, I. S. Bhullar, J. Theprungsirikul, S. K. Davey, H. L. Lim, Y. J. Chiu, and S. Varghese, "3D cardiac μ tissues within a microfluidic device with real-time contractile stress readout," Lab Chip **16**(1), 153–162 (2016).
[34]A. Marsano, C. Conficconi, M. Lemme, P. Occhetta, E. Gaudiello, E. Votta, and M. Rasponi, "Beating heart on a chip: a novel microfluidic platform to generate functional 3D cardiac microtissues," Lab Chip **16**(3), 599–610 (2016).
[35]A. Mathur, P. Loskill, K. Shao, N. Huebsch, S. Hong, S. G. Marcus, and K. E. Healy, "Human iPSC-based cardiac microphysiological system for drug screening applications," Sci. Rep. **5**, 8883 (2015).
[36]A. Agarwal, J. A. Goss, A. Cho, M. L. McCain, and K. K. Parker, "Microfluidic heart on a chip for higher throughput pharmacological studies," Lab Chip **13**(18), 3599–3608 (2013).
[37]Y. K. Kurokawa and S. C. George, "Tissue engineering the cardiac microenvironment: Multicellular microphysiological systems for drug screening," Adv. Drug Delivery Rev. **96**, 225–233 (2016).
[38]X. Lian, J. Zhang, S. M. Azarin, K. Zhu, L. B. Hazeltine, X. Bao, and S. P. Palecek, "Directed cardiomyocyte differentiation from human pluripotent stem cells by modulating Wnt/β-catenin signaling under fully defined conditions," Nat. Protoc. **8**(1), 162–175 (2013).
[39]C. Patsch, L. Challet-Meylan, E. C. Thoma, E. Urich, T. Heckel, J. F. O'Sullivan, and Y. Xia, "Generation of vascular endothelial and smooth muscle cells from human pluripotent stem cells," Nat. Cell Biol. **17**(8), 994 (2015).
[40]J. W. Nichol, S. T. Koshy, H. Bae, C. M. Hwang, S. Yamanlar, and A. Khademhosseini, "Cell-laden microengineered gelatin methacrylate hydrogels," Biomaterials **31**(21), 5536–5544 (2010).
[41]J. Casey, X. Yue, D. Nguyen, A. Acun, V. Zellmer, S. Zhang, and P. Zorlutuna, "3D hydrogel-based microwell arrays as a tumor microenvironment model to study breast cancer growth," Biomed. Mater. (published online 1 February 2017).
[42]D. Zhang, X. Shen, and X. Qi, "Resting heart rate and all-cause and cardiovascular mortality in the general population: a meta-analysis," Can. Med. Assoc. J. **188**(3), E53–E63 (2015).
[43]A. Acun and P. Zorlutuna, "Engineered myocardium model reveals the roles of Hif-1α and HIF1A-AS1 in surviving pathological level oxidative stress," Biomaterials (submitted).
[44]A. G. Koutsiaris, S. V. Tachmitzi, N. Batis, M. G. Kotoula, C. H. Karabatsas, E. Tsironi, and D. Z. Chatzoulis, "Volume flow and wall shear stress quantification in the human conjunctival capillaries and post-capillary venules *in vivo*," Biorheology **44**(5–6), 375–386 (2007).
[45]K. Nimura, M. Yamamoto, M. Takeichi, K. Saga, K. Takaoka, N. Kawamura, and R. J. Schwartz, "Regulation of alternative polyadenylation by Nkx2-5 and Xrn2 during mouse heart development," eLife **5**, e16030 (2016).
[46]J. Hoff, W. Wehner, and V. Nambi, "Troponin in cardiovascular disease prevention: Updates and future direction," Curr. Atheroscler. Rep. **18**(3), 1–9 (2016).
[47]G. T. Dempsey, K. W. Chaudhary, N. Atwater, C. Nguyen, B. S. Brown, J. D. McNeish, and J. M. Kralj, "Cardiotoxicity screening with simultaneous optogenetic pacing, voltage imaging and calcium imaging," J. Pharmacol. Toxicol. Methods **81**, 240–250 (2016).
[48]S. P. Sheehy, F. Pasqualini, A. Grosberg, S. J. Park, Y. Aratyn-Schaus, and K. K. Parker, "Quality metrics for stem cell-derived cardiac myocytes," Stem Cell Rep. **2**(3), 282–294 (2014).
[49]O. Caspi, I. Itzhaki, I. Kehat, A. Gepstein, G. Arbel, I. Huber, and L. Gepstein, "In vitro electrophysiological drug testing using human embryonic stem cell derived cardiomyocytes," Stem Cells Dev. **18**(1), 161–172 (2009).
[50]L. Zwi, O. Caspi, G. Arbel, I. Huber, A. Gepstein, I. H. Park, and L. Gepstein, "Cardiomyocyte differentiation of human induced pluripotent stem cells," Circulation **120**(15), 1513–1523 (2009).
[51]D. A. Pijnappels, M. J. Schalij, A. A. Ramkisoensing, J. van Tuyn, A. A. de Vries, A. van der Laarse, and D. E. Atsma, "Forced alignment of mesenchymal stem cells undergoing cardiomyogenic differentiation affects functional integration with cardiomyocyte cultures," Circ. Res. **103**(2), 167–176 (2008).

[52]D. G. Belair, J. A. Whisler, J. Valdez, J. Velazquez, J. A. Molenda, V. Vickerman, and J. A. Thomson, "Human vascular tissue models formed from human induced pluripotent stem cell derived endothelial cells," Stem Cell Rev. Rep. **11**(3), 511–525 (2015).
[53]M. P. Pusztaszeri, W. Seelentag, and F. T. Bosman, "Immunohistochemical expression of endothelial markers CD31, CD34, von Willebrand factor, and Fli-1 in normal human tissues," J. Histochem. Cytochem. **54**(4), 385–395 (2006).
[54]D. Vestweber, "VE-cadherin the major endothelial adhesion molecule controlling cellular junctions and blood vessel formation," Arterioscler., Thromb., Vasc. Biol. **28**(2), 223–232 (2008).
[55]M. Zhang and A. M. Shah, "ROS signalling between endothelial cells and cardiac cells," Cardiovasc. Res. **102**(2), 249–257 (2014).
[56]D. A. Narmoneva, R. Vukmirovic, M. E. Davis, R. D. Kamm, and R. T. Lee, "Endothelial cells promote cardiac myocyte survival and spatial reorganization implications for cardiac regeneration," Circulation **110**(8), 962–968 (2004).
[57]P. C. Hsieh, M. E. Davis, L. K. Lisowski, and R. T. Lee, "Endothelial-cardiomyocyte interactions in cardiac development and repair," Annu. Rev. Physiol. **68**, 51 (2006).
[58]T. M. Leucker, M. Bienengraeber, M. Muravyeva, I. Baotic, D. Weihrauch, A. K. Brzezinska, and P. F. Pratt, "Endothelial–cardiomyocyte crosstalk enhances pharmacological cardioprotection," J. Mol. Cell. Cardiol. **51**(5), 803–811 (2011).
[59]U. Broeckel, "What can hiPSC-cardiomyocytes teach us about modeling complex human disease phenotypes?," Cell Stem Cell **19**(3), 282–284 (2016).